Light of Two Atoms in Free Space: Bunching or Antibunching?

Sebastian Wolf,[1,*,†] Stefan Richter,[2,3] Joachim von Zanthier,[2,3] and Ferdinand Schmidt-Kaler[1,†]
[1]QUANTUM, Institut für Physik, Johannes Gutenberg-Universität Mainz, Staudingerweg 7, 55128 Mainz, Germany
[2]Institut für Optik, Information und Photonik, Friedrich-Alexander Universität Erlangen-Nürnberg, Staudtstraße 1, 91058 Erlangen, Germany
[3]Erlangen Graduate School in Advanced Optical Technologies (SAOT), Friedrich-Alexander Universität Erlangen-Nürnberg, Paul-Gordan-Straße 6, 91052 Erlangen, Germany

(Received 2 December 2019; accepted 27 January 2020; published 13 February 2020)

Photon statistics divides light sources into three different categories, characterized by bunched, antibunched, or uncorrelated photon arrival times. Single atoms, ions, molecules, or solid state emitters display antibunching of photons, while classical thermal sources exhibit photon bunching. Here we demonstrate a light source in free space, where the photon statistics depends on the direction of observation, undergoing a continuous crossover between photon bunching and antibunching. We employ two trapped ions, observe their fluorescence under continuous laser light excitation, and record spatially resolved the autocorrelation function $g^{(2)}(\tau)$ with a movable Hanbury Brown and Twiss detector. Varying the detector position we find a minimum value for antibunching, $g^{(2)}(0) = 0.60(5)$ and a maximum of $g^{(2)}(0) = 1.46(8)$ for bunching, demonstrating that this source radiates fundamentally different types of light alike. The observed variation of the autocorrelation function is understood in the Dicke model from which the observed maximum and minimum values can be modeled, taking independently measured experimental parameters into account.

DOI: 10.1103/PhysRevLett.124.063603

Hanbury Brown and Twiss were the first to measure the arrival times of photons emitted by classical sources, i.e., from arc lamps and stars, and found that the normalized autocorrelation function $g^{(2)}(\tau)$ for thermal light takes a value of 2 for zero time delay, thus observing photon bunching [1,2]. By contrast, for a single-photon source like a single atom, ion, molecule, or solid state emitter antibunching is observed with $g^{(2)}(0) = 0$, as after the release of a photon the reexcitation of the emitter takes time [3]. This was observed with single atoms, ions, and solid state emitters [4–7]. Arrays of quantum emitters, however, are predicted to show even more fascinating free-space radiation properties resulting from emitter configurations in either superradiant or subradiant states [8–10]. Only if the spatial radiation properties of the ensemble are averaged out, e.g., by collecting a large solid angle into the detector, those features wash out and as a reminder the contrast of superradiance and subradiance is reduced. Yet the spatial dependence of $g^{(2)}(\tau)$ for two identical indistinguishable and immobile single-photon emitters in free space has not been measured so far: what autocorrelation function will be detected?

It turns out that $g^{(2)}$ depends on the angle of observation and may vary between bunched (i.e., super-Poissonian), uncorrelated (Poissonian) and antibunched (i.e., sub-Poissonian) photon statistics. Here we show experimentally that the spatially resolved autocorrelation function $g^{(2)}(0)$ of a pair of ions varies indeed in space and can take values below, above, and equal to 1. Moreover, we find that interference fringes of the intensity correlation function $g^{(2)}(0)$ are phase shifted by π with respect to the intensity interference pattern $G^{(1)}(0)$.

In this Letter we start to outline the quantum description of emission from a pair of indistinguishable emitters [11,12], using the Dicke model, resulting in an analytic expression of the spatial dependence of $g^{(2)}(\boldsymbol{r}, 0)$. Then we describe the experimental apparatus including the movable Hanbury Brown and Twiss detector, and discuss the measured autocorrelation function. Finally, we explain the observed minimal and the observed maximal value of $g^{(2)}(0)$ from independently determined experimental parameters and sketch future application and research goals.

Theory—A pair of identical two-level atoms is advantageously described in the Dicke model [11,12], with symmetric and antisymmetric combinations of the ground states $|g\rangle_i$ and excited states $|e\rangle_i$ of the two atoms, $i = 1, 2$. For an interatomic separation $d \gg \lambda$ and negligible interactions the Dicke states read [see Fig. 1(a)]

$$|e,e\rangle, \qquad |g,g\rangle,$$
$$|s\rangle = \frac{1}{\sqrt{2}}(|e,g\rangle + |g,e\rangle),$$
$$|a\rangle = \frac{1}{\sqrt{2}}(|e,g\rangle - |g,e\rangle).$$

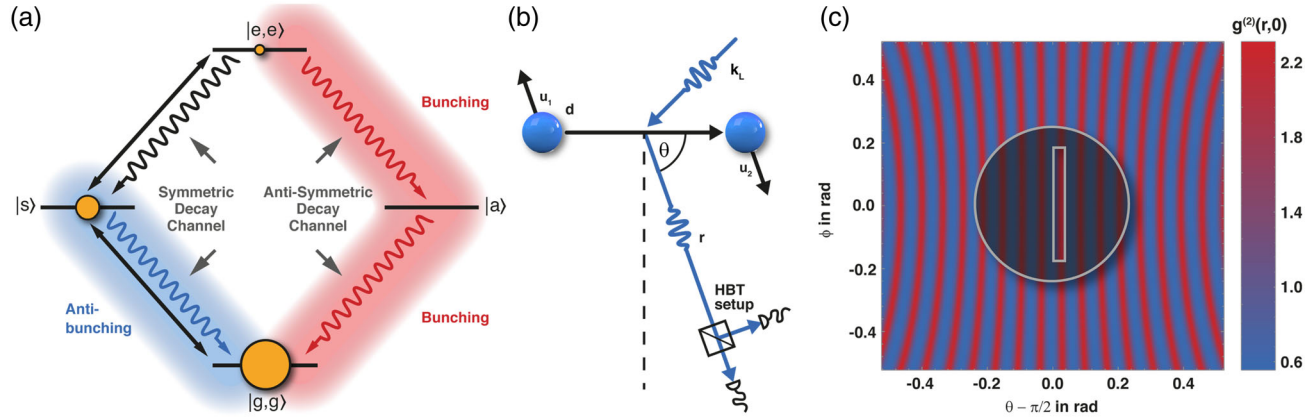

FIG. 1. (a) Dicke model of two identical two-level atoms: Out of the four states $|g,g\rangle$, $|s\rangle = (|e,g\rangle + |g,e\rangle)/\sqrt{2}$, $|a\rangle = (|e,g\rangle - |g,e\rangle)/\sqrt{2}$, $|e,e\rangle$, the states $|g,g\rangle$, $|s\rangle$, and $|e,e\rangle$ are symmetric and the state $|a\rangle$ is antisymmetric. Laser light (black double arrows) couples only the symmetric Dicke states and transfers population (indicated by the size of yellow circles) between $|g,g\rangle \leftrightarrow |s\rangle$ and $|s\rangle \leftrightarrow |e,e\rangle$, whereas spontaneous emission of a photon (shown as curly arrows) connects symmetric states (along symmetric decay channels) as well as antisymmetric states (along antisymmetric decay channels). (b) Because of the trapping potential and the mutual Coulomb repulsion, two ions are fixed in space at a distance $\boldsymbol{d}$. For the measurement of $g^{(2)}(\boldsymbol{r},\tau)$ the two-ion crystal is illuminated with a laser propagating along $\boldsymbol{k}_L$. Scattered photons are recorded in the far field by a spatial-resolving Hanbury Brown and Twiss setup under angle θ. (c) Expected spatial modulation of $g^{(2)}(\boldsymbol{r},\tau)$: regions with photon bunching $g^{(2)}(\boldsymbol{r},\tau) > 1$ (red) alternate with regions with photon antibunching $g^{(2)}(\boldsymbol{r},\tau) < 1$ (blue). As the detection occurs in the plane with azimuthal angle $\phi = 0$ we select the regions by a rectangular slit (white rectangle). Averaging over the full solid angle of the light collection system (white circle) would wash out the spatial variation of $g^{(2)}(\boldsymbol{r},\tau)$.

Because of destructive interference, the dipole interaction with the laser vanishes for the antisymmetric Dicke state. Thus, population is transferred by the laser only between states $|g,g\rangle \leftrightarrow |s\rangle$ and $|s\rangle \leftrightarrow |e,e\rangle$. By contrast, in the limit $d \gg \lambda$, the states $|e,e\rangle$ and $|g,g\rangle$ are connected to the symmetric and the antisymmetric Dicke states alike [see Fig. 1(a)]. Yet, it turns out that the transition amplitude depends on the position of observation. This can be seen when considering the photon detection operator [11]

$$\hat{D} = \hat{\sigma}_1 + e^{i\delta(\boldsymbol{r})}\hat{\sigma}_2, \tag{1}$$

expressing by use of the individual atomic lowering operators $\hat{\sigma}_1 = |g\rangle_1\langle e|$ ($\hat{\sigma}_2 = |g\rangle_2\langle e|$) for atom 1 (atom 2) the two options that either the first or the second atom emits a photon via spontaneous decay. Since it is assumed that the photon detection occurs in the far field, the detector cannot distinguish between these two possibilities, hence both options are considered in Eq. (1). The operator $\hat{D}$ takes further into account the difference in optical phase $\delta(\boldsymbol{r}) = (\boldsymbol{k}_L - k\hat{\boldsymbol{r}}) \cdot \boldsymbol{d} = \boldsymbol{k}_L \cdot \boldsymbol{d} - kd\cos\theta$ between the two possibilities, accumulated by a photon when scattered by atom 1 with respect to a photon scattered by atom 2. Here, $\boldsymbol{k}_L$ is the wave vector of the incoming laser beam, $k = 2\pi/\lambda \approx k_L$ and λ are the wave number and wavelength of the spontaneously emitted photon, respectively, $\boldsymbol{d}$ the distance vector between the two atoms, $\hat{\boldsymbol{r}}$ the unit vector pointing towards the detector at $\boldsymbol{r}$, and θ the polar angle with respect to the ion crystal axis [see Fig. 1(b)].

If the detector is placed at a position δ_s such that $\delta(\boldsymbol{r})$ is an even integer multiple of π the detection operator $\hat{D}$ is symmetric and thus connects only the symmetric Dicke states. For low laser intensities most of the atomic population resides in the ground state $|g,g\rangle$, whereas the state $|s\rangle$ is only little populated and the state $|e,e\rangle$ is hardly occupied at all. Hence, a spontaneously emitted photon will most likely stem from state $|s\rangle$, going along with the transition $|s\rangle \rightarrow |g,g\rangle$ [see Fig. 1(a)]. The dynamics of the laser-driven two-atom system within the four levels of the Dicke model thus takes place essentially between the two levels $|g,g\rangle \leftrightarrow |s\rangle$, resulting in *antibunching* of the emitted photon stream, as for a single two-level atom. However, if the detector is located at a position δ_a such that $\delta(\boldsymbol{r})$ is an odd integer multiple of π, the detection operator $\hat{D}$ becomes antisymmetric. Now, photon detection originates exclusively from the decay channel $|e,e\rangle \rightarrow |a\rangle$, followed by $|a\rangle \rightarrow |g,g\rangle$ thus resulting in bunching of photons in pairs. Single photon events are excluded, because the antisymmetric state $|a\rangle$ cannot be populated by the driving laser field from the ground state $|g,g\rangle$ due to quantum interference [see Fig. 1(a)]. In conclusion, the emission of a two-ion crystal features a remarkable change in photon statistics. Just by moving the detector from δ_s to δ_a, the autocorrelation function varies between antibunching and bunching, while all parameters of the source are kept unchanged.

The detailed calculation shows that the spatial dependence of the autocorrelation function $g^{(2)}(\boldsymbol{r},\tau)$ at $\tau = 0$ for two immobile laser driven two-level atoms is given by [11]

$$g^{(2)}(\boldsymbol{r},0)=\frac{(1+s)^2}{[1+s+\cos\delta(\boldsymbol{r})]^2}, \tag{2}$$

where s denotes the laser saturation of the transition $|g\rangle_i \leftrightarrow |e\rangle_i$ (assumed to be identical for both atoms $i=1,2$). The function $g^{(2)}(\boldsymbol{r},0)$ displays a spatial modulation with a minimal value <1 at δ_s and a maximal value >1 at δ_a. The modulation of $g^{(2)}(\boldsymbol{r},0)$ reveals that the light emitted by a two-ion crystal displays a fundamentally different behavior than the light emitted by a single atom. While the latter exhibits solely antibunching, independent of the angle of observation, the former varies in space, undergoing a continuous crossover from antibunching to laserlike emission of uncorrelated photons, to photon bunching.

The modulation of $g^{(2)}(\boldsymbol{r},0)$ reveals further that the photon statistics of the two-atom system can be tailored via measurement of emitted photons, preparing, moreover, the atomic system into particular entangled states. For example, recording a photon along the direction for the antisymmetric decay channel projects the system into the maximally entangled antisymmetric state $|a\rangle$. We are selecting this projective measurement in free space [13]. For the case of qubits in waveguide structures, the phenomenon has been studied theoretically [14], because it is useful for generating entanglement of distant qubits, e.g., for quantum repeaters [15–20].

Experiment.—In order to reveal the features of the autocorrelation function outlined above, we trap and laser cool two $^{40}Ca^+$ ions in a segmented linear Paul trap [21]. The ions form a linear crystal along the z axis of the trap [trap frequencies $\omega_{z,R1,R2}/2\pi=(0.760,1.275,1.568)$ MHz] with interatomic distance $d=6.7$ μm. Doppler cooling is employed with a laser near 397 nm, red detuned by $2\pi\times 30$ MHz with respect to the $S_{1/2}\rightarrow P_{1/2}$ transition (linewidth of $\Gamma=2\pi\times 22$ MHz [22]). The orientation of its $\boldsymbol{k}_L$ vector allows for continuous cooling of all eigenmodes of the crystal, see Fig. 2. Doppler cooling results in a residual motion of the ions of $\Delta x<100$ nm. A magnetic field of 0.62 mT along the y direction, generated by three pairs of coils, defines the quantization axis. The fluorescence light emitted by the ions is collected with a $f/1.6$ objective at a working distance of 48.5 mm [23]. To resolve the spatial variation of $g^{(2)}(\boldsymbol{r},\tau)$, a movable vertical 1 mm slit aperture behind the objective is introduced, blocking all fluorescence light except for a small angle [see Fig. 1(c)].

The vertical sheet of fluorescence light reflected by a beam splitter, is imaged onto a pinhole with diameter 200 μm to reduce residual background. Indistinguishability of the photon polarization is ensured by introducing a polarizing filter behind the pinhole, transmitting π-polarized light only. The light, after passing a bandpass filter at 400 nm, is fed into a Hanbury Brown and Twiss setup, consisting of a beam splitter and two fiber-coupled

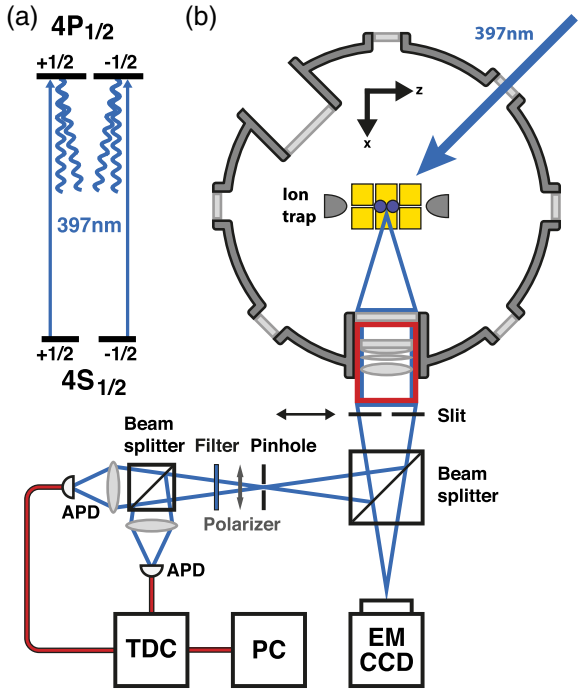

FIG. 2. (a) Relevant level scheme of the $^{40}Ca^+$ $S_{1/2}\rightarrow P_{1/2}$ transition at $\lambda=397$ nm used in the experiment, including Zeeman sublevels. (b) Experimental setup: Two ions, held in a segmented microtrap (yellow), are illuminated by a laser near 397 nm, forming a linear crystal along the z axis of the trap. The fluorescence light is collected by an imaging objective. A movable slit aperture limits the observation to a small solid angle to allow for the discrimination of different observation directions. The light is focused into a Hanbury Brown and Twiss setup.

single-photon avalanche photo diodes (APD) with 85% detection efficiency at 397 nm, dark count rate of 10 Hz, and timing jitter of 1.6 ns. Time tags for each photon detection event are recorded by a time-to-digital converter (TDC) and subsequently correlated via software on a PC.

Automatic data acquisition.—To prevent false data acquisition, a 90:10 beam splitter behind the 1 mm slit aperture transmits 10% of the scattered light to image the two-ion crystal on an electron-multiplying charge coupled device camera (EMCCD), see Fig. 2. In this way the number of ions is constantly monitored using a fluorescence threshold technique. Upon ion loss, the measurement is automatically interrupted, and exactly two ions are reloaded into the trap. Only then, the data acquisition is continued. A 24/7 operation is crucial for obtaining sufficient statistics. Within an acquisition time of 72 h, about 300 correlation events per 2 ns bin were collected for each position over a temporal window of 600 ns.

Results.—Prior to each measurement point of the $g^{(2)}(\boldsymbol{r},\tau)$ signal, the position of the intensity fringe pattern is checked by integrating the added signal from both APDs over 1 min for different slit positions, moved by a micrometer screw. In this way $G^{(1)}$ is obtained, and its

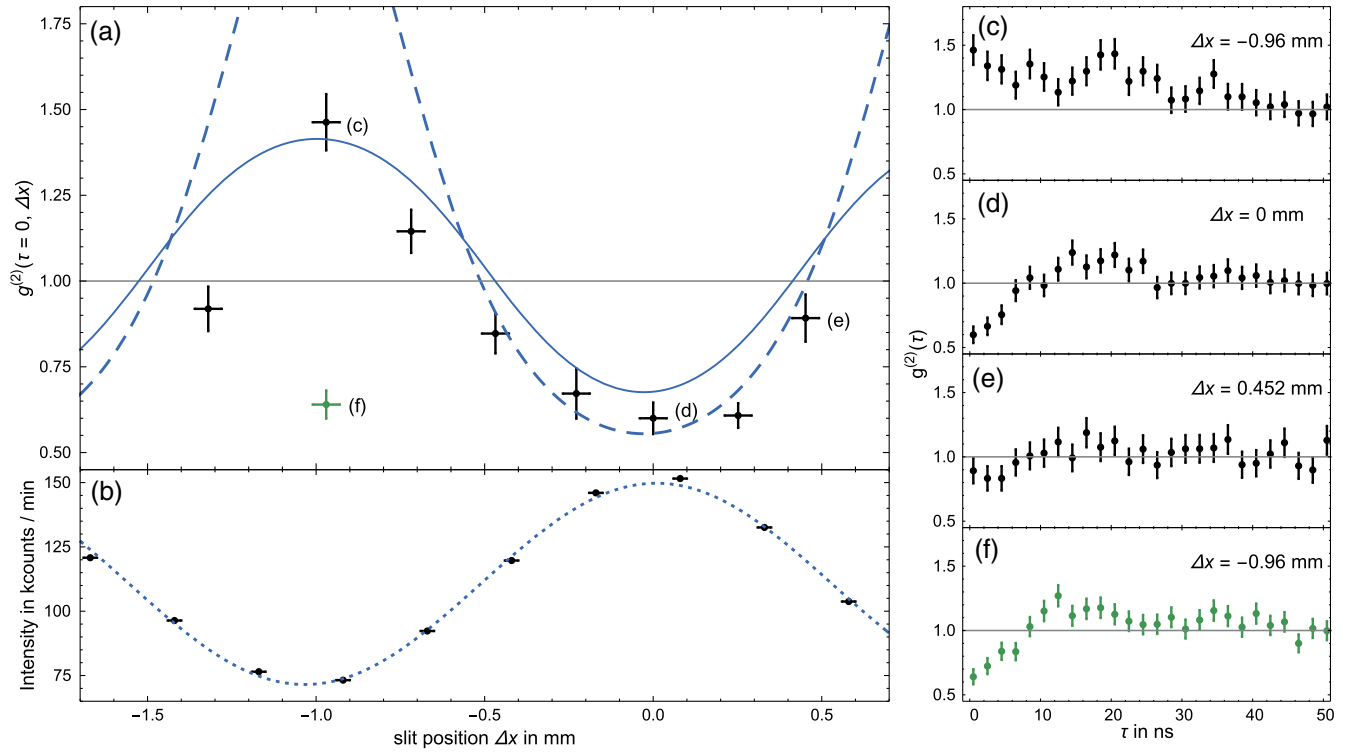

FIG. 3. (a) Experimental results of the two-photon autocorrelation function $g^{(2)}(\boldsymbol{r}, 0)$ for eight different detector positions. The different regimes (bunching, laserlike, antibunching) can be clearly observed. Antibunching is observed in the forward direction, i.e., for a slit position $\Delta x = 0$ mm, where coherent scattering and the intensity interference pattern $G^{(1)}(0)$ [see (b)] take a maximum [23,24]. (c)–(e): temporal dependence of $g^{(2)}(\boldsymbol{r}, \tau)$ for bunched (c), antibunched (d), and laserlike (e) photon statistics for a time window of 600 ns with 2 ns bin size. Taking into account the laser saturation parameter $s = 0.46$ on the $^{40}Ca^{+}$ $S_{1/2} \rightarrow P_{1/2}$ transition and the residual motion of the atoms after Doppler cooling, a spatial modulation of $g^{(2)}(\boldsymbol{r}, \tau)$ as indicated by the blue dashed line is predicted. Considering additionally the multilevel structure of $^{40}Ca^{+}$, i.e., the possible decay into the metastable $3^2D_{3/2}$ level, as well as dark counts and the limited spatial and temporal resolution of the detection process, leads to a modified contrast $g^{(2)}(\boldsymbol{r}, 0)$ (solid line). (f) By altering the inter-ion distance the observed $g^{(2)}(\boldsymbol{r}, 0)$ value changes from bunching to antibunching.

signal periodicity is fitted. The slit position in Figs. 3(a) and 3(b) is given as an offset to the position of the interference maximum of the $G^{(1)}$ signal. The horizontal error bars of $g^{(2)}$ data points [Fig. 3(a)] are obtained from the $G^{(1)}$-fit error. The arrangement allows for determining the spatial and temporal dependence of the autocorrelation function $g^{(2)}(\boldsymbol{r}, \tau)$. The latter was measured at eight different observation angles.

For a slit position of 0 mm, corresponding to $\delta(\boldsymbol{r}) = \delta_s$, we measure $g^{(2)}(\boldsymbol{r}, \tau) = 0.60(5)$, i.e., antibunched photon statistics. However, at $\Delta x = -0.97$ mm, corresponding to $\delta(\boldsymbol{r}) = \delta_a$, we record $g^{(2)}(\boldsymbol{r}, \tau) = 1.46(8)$, i.e., bunched photon statistics. For intermediate positions we find values in between bunching and antibunching. Thus we report values of $g^{(2)}$ which indicate a continuous variation between bunched, uncorrelated, and antibunched photon arrival times. Three examples of different *temporal* emission characteristics are plotted in Figs. 3(c)–3(e). Note that we vary only the angle of observation while keeping all parameters of the light source, i.e., the two-ion crystal, such as laser power, detuning, trap frequency, etc., unchanged.

An alternative way for tailoring the photon statistics of the two-ion crystal is a change of the inter-ion distance. This varies the optical phase difference $\delta(\boldsymbol{r})$, even while the observation angle remains unchanged. Reducing the axial trap frequency ω_z from 760 to 718 kHz, the ion distance increases to $d = 6.97$ μm and δ by 0.96π. Now, the two-photon autocorrelation function switches to antibunching, with $g^{(2)} = 0.64(4)$ [see green data point in Figs. 3(a) and 3(f)].

Our aim is to understand the experimental data from a complete model and fully independently determined parameters: The saturation parameter s is measured via the autocorrelation of the light scattered by a single ion allowing for the observation of Rabi oscillations. From the frequency of $g^{(2)}$ oscillations and the measured detuning $\Delta = 2\pi \times 30(3)$ MHz of the excitation laser, the saturation parameter is determined [5] (Fig. 4) to $s = 0.46(8)$. Near resonance, with $\Gamma/\Delta \sim 1$, Eq. (2) derived for resonant excitation holds. The ion motion, after Doppler cooling with a phonon number in every mode of $n \approx 10$ is leading to a Debye-Waller-Factor $f_{\mathrm{DW}} = 0.50(5)$. The spatial

periodicity of the $g^{(2)}$ signal is determined as $L = 1.94(4)$ mm, using the $G^{(1)}$ signal of a two-ion crystal. This model leads to the prediction shown in Fig. 3(a) (dashed line), with only the horizontal offset as a fit parameter. The obtained phase shift between $g^{(2)}$ and $G^{(1)}$ is $1.033(11)\,\pi$, in agreement with the expected value of π.

A maximum of $g^{(2)}_{\mathrm{max}}(0) = 2.31(27)$ is expected for bunching and $g^{(2)}_{\mathrm{min}}(0) = 0.55(03)$ for antibunching, respectively. Including additional mechanisms limiting the achievable $g^{(2)}$ contrast refines the model and improves the agreement with the measured data. Equation (2) is derived from a theory based on two-level atoms. Yet, $^{40}Ca^{+}$ has a more complex level structure. If the ions decay into the metastable $3D_{3/2}$-level (branching ratio $\sim 1:16$ [22]), only a single ion remains in the trap that may scatter photons at 397 nm, now showing perfect antibunching. Additionally, the slit has a finite width of 1 mm to collect a sufficient number of photons. This leads to an averaging of the $g^{(2)}$ signal over this spatial detection angle, further reducing the contrast. Also, the temporal uncertainty of 1.6 ns of the employed photo detectors averages the temporal behavior of the ions, governed by an exponential decay towards $g^{(2)}(\tau) = 1$ with a time constant given by the excited state lifetime of $\tau = 6.9$ ns [22]. Finally, the dark count rate of the detectors leads to false start and stop signals of the $g^{(2)}$ measurement giving rise to a constant offset of the $g^{(2)}$ signal. When summarized, the listed effects lead to $g^{(2)}_{\mathrm{max}}(0) = 1.41(12)$ for bunching and $g^{(2)}_{\mathrm{min}}(0) = 0.68(2)$ for antibunching, respectively [see blue solid line in Fig. 3(a)]. Taking into account the eight measured values in Fig. 3(a), we find good agreement with the expected spatial modulation of $g^{(2)}(\boldsymbol{r}, \tau)$, derived from the independent evaluation.

The photon correlation signal for the ion crystal may be further improved by following a strategy for the light collection after the pinhole known as Köhler illumination in classical microscopy. In this way the light collection can be optimized while still keeping a far-field observation situation for the ions in the crystal such that emitted photons remain fully indistinguishable.

In the future, we plan spatiotemporal two-photon correlation measurements with increased contrast allowing for the observation of superbunching [25]. We further anticipate impact of our method for quantum computing [26–28] and quantum communication [29,30], when distant processor units are connected via projective measurements [13,15–20], possibly also for larger ion crystals [31–34]. The measured heralded quantum entanglement of states can also be converted to a tailored decay yielding long-lived entangled spin states. A designed photon statistics allows furthermore for improved imaging techniques, useful in the life sciences [35–37]. Measuring cross-correlations instead of autocorrelations may finally disclose the nonclassicality of the photon correlations [38], applicable for ultraprecise sensing, intensity interferometry [6,11,12,39], and structure analysis in crystallography [40].

S. R. and J. v. Z. acknowledge support from the Graduate School of Advanced Optical Technologies (SAOT), Erlangen and the International Max-Planck Research School, Physics of light, Erlangen.

*wolfs@uni-mainz.de
†http://www.quantenbit.de

[1] R. H. Brown and R. Q. Twiss, Correlation between photons in two coherent beams of light, Nature (London) **177**, 27 (1956).
[2] R. H. Brown and R. Twiss, A test of a new type of stellar interferometer on Sirius, Nature (London) **178**, 1046 (1956).
[3] R. Loudon, *The Quantum Theory of Light* (OUP, Oxford, 2000).
[4] H. J. Kimble, M. Dagenais, and L. Mandel, Photon Antibunching in Resonance Fluorescence, Phys. Rev. Lett. **39**, 691 (1977).
[5] F. Diedrich and H. Walther, Nonclassical Radiation of a Single Stored Ion, Phys. Rev. Lett. **58**, 203 (1987).
[6] T. Basché, W. E. Moerner, M. Orrit, and H. Talon, Photon Antibunching in the Fluorescence of a Single Dye Molecule Trapped in a Solid, Phys. Rev. Lett. **69**, 1516 (1992).
[7] I. Aharonovich, D. Englund, and M. Toth, Solid-state single-photon emitters, Nat. Photonics **10**, 631 (2016).
[8] M. O. Scully, E. S. Fry, C. H. Raymond Ooi, and K. Wódkiewicz, Directed Spontaneous Emission from an Extended Ensemble of N Atoms: Timing Is Everything, Phys. Rev. Lett. **96**, 010501 (2006).
[9] R. Wiegner, J. von Zanthier, and G. S. Agarwal, Quantum-interference-initiated superradiant and subradiant emission from entangled atoms, Phys. Rev. A **84**, 023805 (2011).
[10] P.-O. Guimond, A. Grankin, D. V. Vasilyev, B. Vermersch, and P. Zoller, Subradiant Bell States in Distant Atomic Arrays, Phys. Rev. Lett. **122**, 093601 (2019).
[11] C. Skornia, J. von Zanthier, G. S. Agarwal, E. Werner, and H. Walther, Nonclassical interference effects in the radiation from coherently driven uncorrelated atoms, Phys. Rev. A **64**, 063801 (2001).
[12] C. Schön and A. Beige, Analysis of a two-atom double-slit experiment based on environment-induced measurements, Phys. Rev. A **64**, 023806 (2001).
[13] C. Thiel, J. von Zanthier, T. Bastin, E. Solano, and G. S. Agarwal, Generation of Symmetric Dicke States of Remote Qubits with Linear Optics, Phys. Rev. Lett. **99**, 193602 (2007).
[14] X. H. H. Zhang and H. U. Baranger, Heralded Bell State of Dissipative Qubits Using Classical Light in a Waveguide, Phys. Rev. Lett. **122**, 140502 (2019).
[15] D. L. Moehring, P. Maunz, S. Olmschenk, K. C. Younge, D. N. Matsukevich, L.-M. Duan, and C. Monroe, Entanglement of single-atom quantum bits at a distance, Nature (London) **449**, 68 (2007).
[16] J. Hofmann, M. Krug, N. Ortegel, L. Gérard, M. Weber, W. Rosenfeld, and H. Weinfurter, Heralded entanglement between widely separated atoms, Science **337**, 72 (2012).

[17] H. Bernien, B. Hensen, W. Pfaff, G. Koolstra, M. S. Blok, L. Robledo, T. Taminiau, M. Markham, D. J. Twitchen, L. Childress *et al.*, Heralded entanglement between solid-state qubits separated by three metres, Nature (London) **497**, 86 (2013).

[18] L. Slodička, G. Hétet, N. Röck, P. Schindler, M. Hennrich, and R. Blatt, Atom-Atom Entanglement by Single-Photon Detection, Phys. Rev. Lett. **110**, 083603 (2013).

[19] A. Delteil, Z. Sun, W.-b. Gao, E. Togan, S. Faelt, and A. Imamoğlu, Generation of heralded entanglement between distant hole spins, Nat. Phys. **12**, 218 (2016).

[20] R. Stockill, M. J. Stanley, L. Huthmacher, E. Clarke, M. Hugues, A. J. Miller, C. Matthiesen, C. Le Gall, and M. Atatüre, Phase-Tuned Entangled State Generation between Distant Spin Qubits, Phys. Rev. Lett. **119**, 010503 (2017).

[21] G. Jacob, K. Groot-Berning, S. Wolf, S. Ulm, L. Couturier, S. T. Dawkins, U. G. Poschinger, F. Schmidt-Kaler, and K. Singer, Transmission Microscopy with Nanometer Resolution Using a Deterministic Single Ion Source, Phys. Rev. Lett. **117**, 043001 (2016).

[22] M. Hettrich, T. Ruster, H. Kaufmann, C. F. Roos, C. T. Schmiegelow, F. Schmidt-Kaler, and U. G. Poschinger, Measurement of Dipole Matrix Elements with a Single Trapped Ion, Phys. Rev. Lett. **115**, 143003 (2015).

[23] S. Wolf, J. Wechs, J. von Zanthier, and F. Schmidt-Kaler, Visibility of Young's Interference Fringes: Scattered Light from Small Ion Crystals, Phys. Rev. Lett. **116**, 183002 (2016).

[24] U. Eichmann, J. C. Bergquist, J. J. Bollinger, J. M. Gilligan, W. M. Itano, D. J. Wineland, and M. Raizen, Young's Interference Experiment with Light Scattered from Two Atoms, Phys. Rev. Lett. **70**, 2359 (1993).

[25] D. Bhatti, J. von Zanthier, and G. S. Agarwal, Superbunching and nonclassicality as new hallmarks of superradiance, Sci. Rep. **5**, 17335 (2015).

[26] L. Jiang, J. M. Taylor, A. S. Sørensen, and M. D. Lukin, Distributed quantum computation based on small quantum registers, Phys. Rev. A **76**, 062323 (2007).

[27] L. Luo, D. Hayes, T. Manning, D. Matsukevich, P. Maunz, S. Olmschenk, J. Sterk, and C. Monroe, Protocols and techniques for a scalable atom–photon quantum network, Fortschr. Phys. **57**, 1133 (2009).

[28] L.-M. Duan and C. Monroe, Colloquium: Quantum networks with trapped ions, Rev. Mod. Phys. **82**, 1209 (2010).

[29] H.-J. Briegel, W. Dür, J. I. Cirac, and P. Zoller, Quantum Repeaters: The Role of Imperfect Local Operations in Quantum Communication, Phys. Rev. Lett. **81**, 5932 (1998).

[30] L.-M. Duan, M. Lukin, J. I. Cirac, and P. Zoller, Long-distance quantum communication with atomic ensembles and linear optics, Nature (London) **414**, 413 (2001).

[31] P. Obšil, A. Lešundák, T. Pham, G. Araneda, M. Čížek, O. Číp, R. Filip, and L. Slodička, Multipath interference from large trapped ion chains, New J. Phys. **21**, 093039 (2019).

[32] T. Richter, Photon correlations in the cooperative radiation from a continuously and incoherently pumped three-atom system, J. Phys. B **15**, 1293 (1982).

[33] S. Oppel, R. Wiegner, G. S. Agarwal, and J. von Zanthier, Directional Superradiant Emission from Statistically Independent Incoherent Nonclassical and Classical Sources, Phys. Rev. Lett. **113**, 263606 (2014).

[34] Qurrat-ul-Ain Gulfam and Z. Ficek, Highly directional photon superbunching from a few-atom chain of emitters, Phys. Rev. A **98**, 063824 (2018).

[35] T. Dertinger, R. Colyer, G. Iyer, S. Weiss, and J. Enderlein, Fast, background-free, 3D super-resolution optical fluctuation imaging (SOFI), Proc. Natl. Acad. Sci. U.S.A. **106**, 22287 (2009).

[36] O. Schwartz, J. M. Levitt, R. Tenne, S. Itzhakov, Z. Deutsch, and D. Oron, Superresolution microscopy with quantum emitters, Nano Lett. **13**, 5832 (2013).

[37] A. Classen, J. von Zanthier, and G. S. Agarwal, Analysis of super-resolution via 3D structured illumination intensity correlation microscopy, Opt. Express **26**, 27492 (2018).

[38] R. Wiegner, C. Thiel, J. von Zanthier, and G. Agarwal, Creating path entanglement and violating Bell inequalities by independent photon sources, Phys. Lett. A **374**, 3405 (2010).

[39] T. Richter, Interference between the resonance fluorescence fields from two independent atoms and spatial two-photon correlations, Opt. Commun. **80**, 285 (1991).

[40] A. Classen, K. Ayyer, H. N. Chapman, R. Röhlsberger, and J. von Zanthier, Incoherent Diffractive Imaging via Intensity Correlations of Hard X Rays, Phys. Rev. Lett. **119**, 053401 (2017).